Progress In Electromagnetics Research, Vol. 121, 281–299, 2011

INTERACTION OF AN ASYMMETRIC SCANNING NEAR FIELD OPTICAL MICROSCOPY PROBE WITH FLUORESCENT MOLECULES

V. Lotito [1, 2, *], U. Sennhauser [1], C. V. Hafner [2], and G.-L. Bona [1, 2]

[1]Electronics/Metrology Laboratory, EMPA, Swiss Federal Laboratories for Materials Science and Technology, Ueberlandstrasse 129, CH-8600 Dübendorf, Switzerland

[2]Department of Information Technology and Electrical Engineering, ETH Zurich, Gloriastrasse 35, 8092 Zurich, Switzerland

Abstract—We present a numerical analysis of the interaction between novel scanning near field optical microscopy probes based on an asymmetric structure and a single fluorescent molecule. Our finite element analysis shows how such near field probes can be effectively used for high resolution detection of single molecules, in particular those with a longitudinal dipole moment. At the same time, fluorescent molecules can be exploited as point-like probes of the single vectorial components of the near field distribution at the probe apex, providing a powerful tool for near field probe characterization.

1. INTRODUCTION

Scanning near field optical microscopy (SNOM) has emerged over the past decades as a powerful technique to get a nanoscale insight into topographical and optical properties of a sample, drawing the attention of scientists for several applications ranging from life to material science [1–4]. A great effort has been devoted throughout the years to the optimization of the near field probe, which plays a major role in the interaction with the sample and in the ultimate attainable resolution [5, 6]. Since the proposal of the pioneering aperture structure, based on a metal coated dielectric with a subwavelength aperture left at the end, different options have been explored in order to overcome some of its fundamental drawbacks, i.e., the poor resolution

Received 17 September 2011, Accepted 17 October 2011, Scheduled 27 October 2011

* Corresponding author: Valeria Lotito (Valeria.Lotito@empa.ch).

limited by the size of the aperture, the low throughput and the asymmetric near field distribution at the probe apex resulting from the linearly polarized excitation [7–9]. Apertureless probes under far field external illumination have been indicated as a possible alternative [10–13]: although they allow the achievement of high field enhancement and high resolution, the far field illumination creates a strong background potentially deleterious for measurements on sensitive samples, as is the case for, e.g., fluorescent molecules.

A viable solution is given by apertureless fully metal-coated tips under internal back excitation. Just as metallic probes under far field external illumination, they allow high field enhancement and strong confinement to an ultra-small spot whose size is mostly limited by the diameter of the metal apex (which can be sharpened at will); at the same time, they pose minor risks for sensitive samples, because of the lack of the strong deleterious background [8, 10, 11, 14–16]. However, such desirable properties can be obtained only under a radially polarized excitation, which unfortunately requires an injection procedure extremely sensitive to misalignments [17]. In fact, the surface plasmon polaritons (SPPs) excited by the radially polarized input on the metal surface interfere constructively at the tip apex, due to the rotational symmetry of both the input polarization and the probe, resulting in a highly localized hot spot, at the basis of nanofocusing; on the contrary, the SPPs excited by a linearly polarized excitation interfere destructively at the tip apex due to the opposite polarities on the opposite sides of the tip, giving rise to a broad, asymmetric and weak near field distribution [16, 18].

In order to circumvent the inconvenience inherent in the use of a radially polarized excitation and get nanofocusing under linearly polarized excitation, it is necessary to break the symmetry of the originally axisymmetric structure. If z is the direction of the probe axis and an asymmetry is introduced in the tip structure along x, field confinement under x linearly polarized mode can be attained, the size and the peak intensity of the achieved spot being dependent on the characteristics of the asymmetry. Different structures have been examined, from modifications in the metal coating like slits and asymmetric corrugations to oblique cuts removing the metal coating and the core of the probe [19–21]: a proper engineering of the asymmetry can lead to spot sizes comparable to those achieved under radially polarized excitation with even better peak intensity values. Therefore, such asymmetric structures could potentially be promising candidates in high resolution SNOM applications and deserve further numerical investigation and experimental validation.

However, the accurate characterization of the near field optical

properties of novel probe structures represents a challenging task. A tip-on-tip or probe-to-probe configuration has been proposed for this purpose [17, 22]: such an arrangement, in which one tip with known properties is used as a probe to collect the near field distribution of the novel tip, requires a good alignment between the two probe axes, which adds to the complexity of the experimental set-up. A more detailed description of the near field pattern at the probe apex can be obtained using single fluorescent molecules. In the seminal work by Betzig and Chichester, fluorescent molecules were used to map the electric field distribution of aperture probes [23]: in fact, a fluorescent molecule can be interpreted as an electrical dipole acting as a point detector for the components of the electric field aligned along its absorption dipole direction, because the emitted fluorescence intensity is proportional to the square of the local electric field parallel to its absorption dipole. As a consequence, this characterization technique provides a precious glimpse into the vectorial components of the electric field distribution close to the tip apex.

The interaction of single fluorescent molecules with aperture probes has been thoroughly analyzed both experimentally and theoretically [24–26]. The interest in such a topic stems not only from its importance as a characterization technique, but also because single molecule detection is a hot issue in biological as well as in material science [1, 27]. A requisite of paramount importance for single fluorescent molecule detection is the reduction of the excitation volume of the molecule in order to discriminate the signal emitted by a single molecule among the signal arising from surrounding molecules, which acts as an interfering background [28]. SNOM looks particularly suitable for this purpose due to the strong localization of the field emitted by the probe; moreover, due to the presence of transverse and longitudinal field components close to the probe apex, it has been used for the determination of the three-dimensional (3D) orientation of single fluorophores by controlling the polarization of the excitation light [29]. Aperture SNOM probes have been employed for fluorescence studies on biological molecules and polymers [24, 28–31].

Contrarily to the vast literature available for aperture probes, a systematic and comprehensive numerical analysis of the interaction of apertureless probes with single fluorescent molecules is still missing, although high resolution in single fluorescent molecule detection has been demonstrated for measurements performed using apertureless probes under internal radially polarized excitation, due to the better field confinement [32]. Furthermore, as anticipated, asymmetric SNOM probes excited with linearly polarized light along the direction of the asymmetry are expected to guarantee field localization with

peak intensity comparable or better than axisymmetric fully metal-coated probes under radially polarized excitation, while enabling a simplification in the injection procedure. Hence, their interaction with single fluorescent molecules is of primary interest as well.

In this paper, we investigate the interaction between novel asymmetric SNOM probes and a single fluorescent molecule. First, the interaction between an axisymmetric fully metal-coated probe under radially polarized excitation and a single fluorescent molecule will be examined. Next, these results will be compared with those obtained in case of asymmetric probes. It will be shown that the vectorial components of the near field emitted by an asymmetric probe under proper linearly polarized excitation closely resemble those of an axisymmetric fully metal-coated probe under radially polarized excitation with the presence of strong longitudinal field components. Hence, on the one hand, single fluorescent molecule detection can be used as a characterization technique to analyze how effective this conversion into a mainly longitudinally polarized emission pattern is for asymmetric probes with different geometric characteristics. On the other hand, asymmetric probes with known near field distribution can be used for single fluorescent molecule detection as an effective substitute for fully metal-coated axisymmetric probes. In this case, the comparison of the experimental fluorescence measurements with our numerical results may aid in the determination of the 3D orientation of single molecules.

2. NUMERICAL MODEL

Due to the lack of analytical solutions for the asymmetric SNOM probes, a numerical approach has been adopted. Using Comsol Multiphysics, a finite element based commercial software, full 3D simulations have been carried out to determine the field distributions close to the probe apex of either axisymmetric fully metal-coated tips or asymmetric probes, by exciting the structure from the bottom with a properly polarized excitation (radial for the axisymmetric tip and linear for the asymmetric ones). Simulations have been run on a 64-bit workstation with 32 GB of RAM using second order elements with minimum size of about 0.8 nm. The modeling domain is a cylinder of radius equal to 1 μm and height of 1.6 μm.

The axisymmetric probe (Figure 1(a)) consists of a silica core ($n = 1.5$) covered by an aluminium coating ($n = 0.645 + 5.029i$ at the operating wavelength of 532 nm). The initial radii of the tapered structure with a 30° full cone angle are 225 nm for the inner core and 275 nm for the outer edge of the metallic hollow cone. Both

the inner silica cone and the aluminium hollow cone have rounded terminations with radii of 10 and 20 nm, respectively. The asymmetric probes consist in the introduction of a proper asymmetric modification in the originally axisymmetric structure (Figure 1(b)): a cut probe was considered due to the simplicity to fabricate this probe using focused ion beam milling, a technique commonly employed for the creation of flat apertures in standard aperture probes. The geometric parameters characterizing this probe are the cut angle (measured between a plane orthogonal to the probe axis and the plane of the cut itself) and the

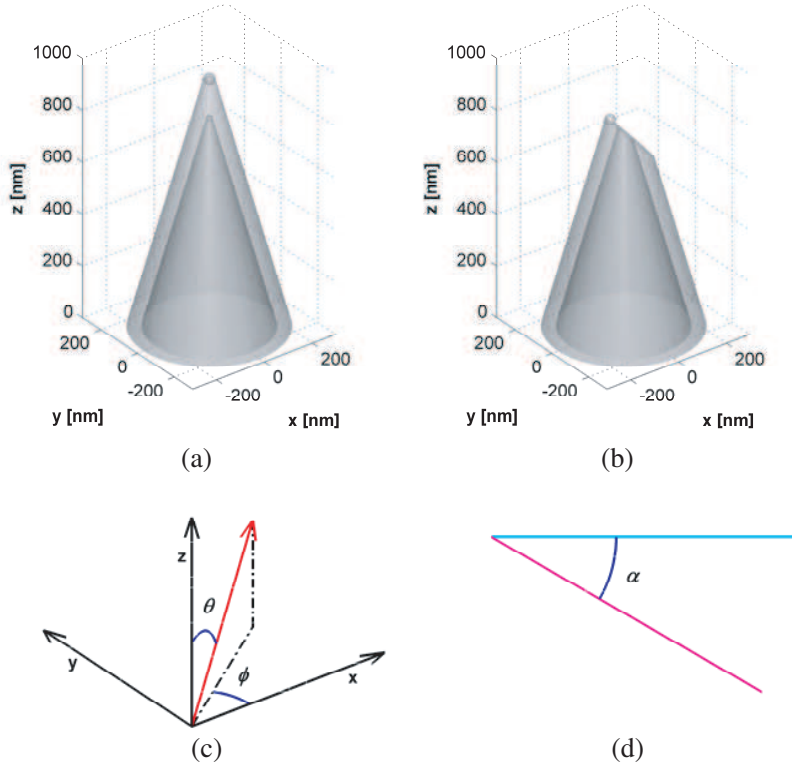

Figure 1. Sketch of the simulated structures: (a) axisymmetric probe; (b) asymmetric cut probe; (c) representation of the orientation of the dipole (red vector) through the polar angle θ and the azimuthal angle ϕ; (d) angle α between the direction of the input linear polarization (indicated by the magenta line) and the direction of the asymmetry (represented with the cyan line); both the lines lie in the xy plane. According to Figure 1(b), the asymmetry is present along the x axis.

cut height (that is, the height of the new probe apex measured from the bottom of the simulated tapered structure).

The interaction with fluorescent molecules with different orientations located at 10 nm from the probe apex has been modeled by recalling that the fluorescence intensity I emitted by a molecule is related to the square of the dot product of the local electric field $\mathbf{E}$ and the normalized absorption dipole moment $\mathbf{p}$ [23]:

$$I \propto |\mathbf{E} \cdot \mathbf{p}|^2 \tag{1}$$

Equation (1) highlights the dependence of the fluorescence intensity I on both the absolute value and the direction of the electric field, thereby explaining the ability of a fluorescent molecule to provide a vectorial picture of the local electric field. The normalized absorption dipole moment which characterizes the 3D dipole orientation can be formulated as:

$$\mathbf{p} = \begin{pmatrix} \sin\theta\cos\phi \\ \sin\theta\sin\phi \\ \cos\theta \end{pmatrix} \tag{2}$$

where θ and ϕ represent the polar and azimuthal angle, respectively (Figure 1(c)). In our case the local field $\mathbf{E} = (E_x, E_y, E_z)$ coincides with the electric field distribution on the xy plane at a distance z of 10 nm above the probe apex. In Figure 1(d), we have also depicted the angle α between the direction of the input linear polarization and the direction along which the asymmetry is present: according to the sketch in Figure 1(b), the asymmetry lies along the x axis. In the following paragraph, the distributions obtained for fluorophores with different orientations for an axisymmetric probe under radially polarized excitation are reported and compared to those obtained for an asymmetric probe under linearly polarized excitation.

3. PROBE-MOLECULE INTERACTION

The axisymmetric probe was excited with a radially polarized excitation, while changing the polar and azimuthal orientation of the fluorescent molecule from 0° to 90° with a step of 30°. The simulated fluorescence intensity distributions calculated according to Equation (1) on a 400 nm by 400 nm square area centered on the probe apex are shown in Figure 2. The number in the upper left corner of each plot indicates the peak intensity for a molecule with a specific dipole orientation normalized to the peak of the total local electric field intensity $|\mathbf{E}|^2$ (square of the norm of the electric field). As apparent, the radially polarized excitation results in a strong longitudinal local field at the tip apex (corresponding to $\theta = 0°$), made up of a single hot

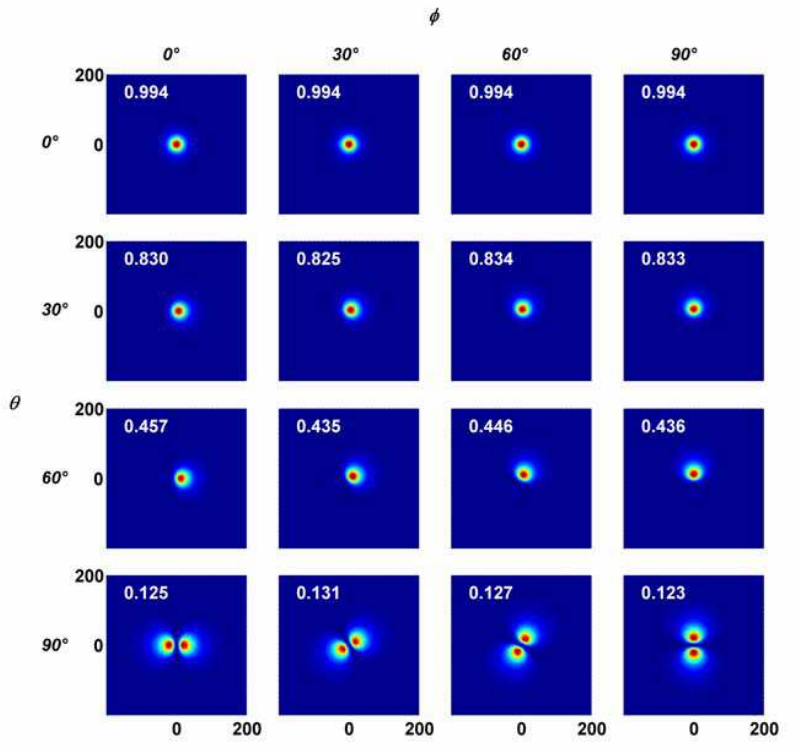

Figure 2. Simulated fluorescence intensity maps over a 400 nm by 400 nm square area for single molecules with different orientations (as specified by the polar angle θ and the azimuthal angle ϕ) excited by an axisymmetric fully metal-coated probe under radially polarized excitation and located at a distance of 10 nm from the tip apex. All the maps are reported on the same color scale, with each plot normalized to its peak intensity value.

spot, and weaker orthogonal transverse components (corresponding to $\theta = 90^\circ$ and $\phi = 0^\circ$ and $\theta = 90^\circ$ and $\phi = 90^\circ$, respectively) of almost equal magnitude appearing as two-lobed patterns. Note that we use the adjective longitudinal for the component aligned along the probe axis z and transverse for those lying in the xy plane. Similarly, we will adopt the same expressions to refer to molecules with a dipole moment either oriented along z or lying in the xy plane.

The calculated field distributions can help in the interpretation of fluorescence measurements and in the determination of the 3D orientation of a fluorescent molecule. Due to the axial symmetry of

both the probe and the input excitation, a variation in the azimuthal angle of the fluorophore does imply almost no change in the peak value and in the overall shape of the intensity distribution, which rotates only its prevalent orientation according to ϕ. On the contrary, a variation of the polar angle θ from 0° to 90° gives rise to a decrease in the peak intensity and a gradual transition from a single spot to a two-lobed distribution, as the dipole absorption moment overlaps dominantly with the weaker transverse components of the local electric field rather than with the stronger longitudinal component. The full width at half maximum (FWHM) varies from about 30 nm for θ between 0° and 60° to a maximum of about 80 nm for a dipole without any longitudinal component ($\theta = 90°$).

Some notable features with respect to aperture probes under usual linearly polarized excitation are worth being pointed out. First, the eloquently distinct dominance of a single lobe longitudinal component in the probe near field distribution marks a striking difference and has important consequences on the imaging of dipoles with a mainly longitudinal dipole moment. These molecules are usually imaged as two lobes with aperture probes, because the longitudinal component of the electric field close to the aperture is strong only on the aperture edge at two diametrically opposite positions aligned along the direction of the input linear polarization. From a practical standpoint, better imaging of molecules with a mainly longitudinal dipole moment (like terylene molecules in p-terphenyl [33] or TRITC-DHPE molecules in DPPC monolayers [24]) could be achieved. Moreover the determination of the orientation of molecules with the same polar angle and different azimuthal orientation becomes easier. In fact, such molecules are imaged almost identically in terms of shape and intensity of the fluorescence pattern with fully metal-coated probes under radially polarized excitation, apart from the rotation by ϕ which allows the determination of the azimuthal component of the fluorophore dipole moment. On the contrary, using aperture probes strong differences in intensities and shape of the field distributions emerge in molecules with variable azimuthal angle due to the significant differences in orthogonal transverse components close to the aperture, with variations in peak intensities by even two orders of magnitude [25]. We should also recall another outstanding advantage of fully metal-coated probes with respect to aperture probes, in that the overall resolution is limited mostly by the size of the metal apex, which can be made smaller holding the promise for better resolution, while the aperture size cannot be decreased at will to avoid a drop in the signal throughput [32].

The interaction with single fluorescent molecules has been

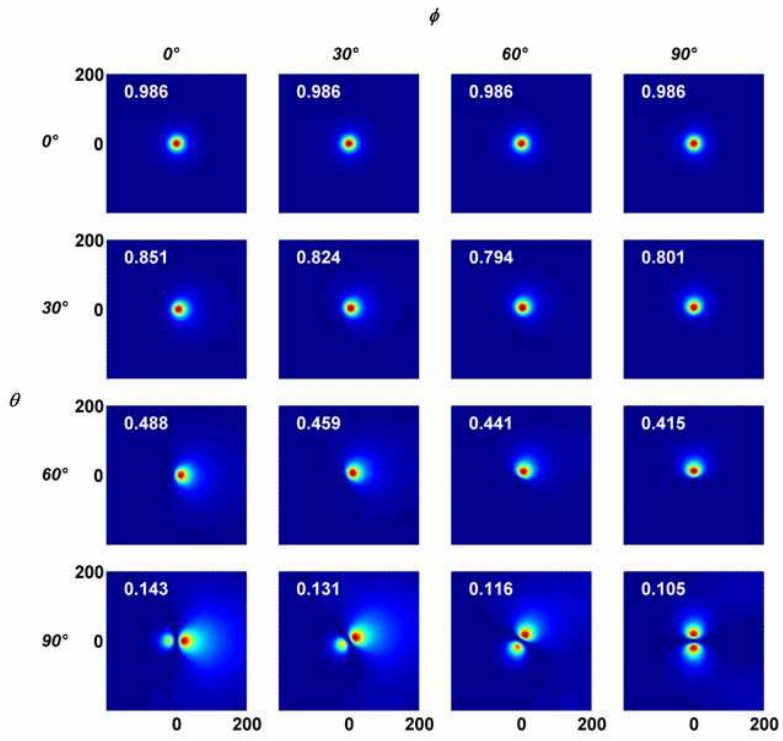

Figure 3. Simulated fluorescence intensity maps over a 400 nm by 400 nm square area for single molecules with different orientations (as specified by the polar angle θ and the azimuthal angle ϕ) excited by a cut probe under linearly polarized excitation along the direction of the asymmetry (x) and located at a distance of 10 nm from the tip apex. All the maps are reported on the same color scale, with each plot normalized to its peak intensity value.

investigated also for an asymmetric probe based on an oblique cut, creating an asymmetry along x. Figure 3 refers to a structure with a cut angle of 30° and a cut height (measured from the bottom of the simulated tapered structure) of 766 nm under x linearly polarized excitation (i.e., oriented along the direction of the asymmetry; $\alpha = 0°$). The dominance of the longitudinal component over the transverse components of the electric field is evident also in this case; the two orthogonal transverse components still exhibit a double-lobed structure, even if they are slightly different in magnitude, as the electric field component aligned along the input linear polarization

direction prevails against the orthogonal one. Therefore, while for the axisymmetric probe under radially polarized excitation almost no change in the fluorescence intensity mapping occurred with the azimuthal angle ϕ at constant polar angle θ, for the asymmetric probe minor variations are observed upon a change of ϕ due to the slight inequality of the two transverse components. However, such negligible variations do not represent a major pitfall: the close resemblance with the fluorescence distributions obtained for an axisymmetric probe under radially polarized excitation is still remarkable, which makes the asymmetric structure a promising alternative to the axisymmetric one for single fluorescent molecule studies, as it offers the advantages pointed out for the axisymmetric probe, but under an easier linearly polarized excitation.

To better emphasize the similarities of the distributions obtained for the axisymmetric and the asymmetric probes, we examined the projections along the $y = 0$ axis for $\phi = 0°$ and variable θ (Figures 4(a) and (b)) and along the straight line $x \cdot \tan(\phi)$ for $\theta = 90°$ and variable ϕ (Figures 4(c) and (d)).

For both the axisymmetric and the asymmetric probes, the fluorescence map becomes two-lobed as the polar angle θ approaches 90° (Figures 4(a) and (b)). In the asymmetric probe (Figure 4(b)) a slight asymmetry appears in the two lobes for $\theta = 90°$ and $\phi = 0°$, but the overall shape as well as the FWHM are similar to the ones of the axisymmetric structure (Figure 4(a)), with the maximum spot size varying from about 30 nm for θ between 0° and 60° to about 74 nm for a dipole without any longitudinal component ($\theta = 90°$). For variations in the azimuthal orientation of the molecule at constant polar angle θ, we get two-lobed patterns for both structures and all azimuthal angles (Figures 4(c) and (d)): in case of the asymmetric probe, we observe small asymmetries between the two lobes and peak fluctuations, but the asymmetry between the lobes gradually vanishes as the dipole moment becomes orthogonal to the input linear polarization (Figure 4(d)).

To study how effective the conversion into a mainly longitudinally polarized distribution is for asymmetric probes with different geometric parameters (cut height and cut angle), the behavior of various probe structures has been examined. As figures of merit for a comparison, the following quantities have been considered (Table 1): first, the ratio of the peak intensity of the longitudinal and transverse components aligned along x and y to the peak intensity of the total electric field; second, the range of variation of the FWHM for fluorescent molecules with longitudinal and transverse dipole moments. In order to highlight the relative magnitude of the total electric field intensity for the

different probe structures, the peak value of the total electric field intensity for each structure normalized to the one of the axisymmetric probe has been reported as well.

It is noteworthy that, independently of the total electric field intensity, all the asymmetric structures exhibit a highly confined strong longitudinal electric field component and weaker transverse components, like the axisymmetric probe under radially polarized excitation. Hence, probes with optimal total intensities can be chosen. As observed, differently from the axisymmetric probe, where orthogonal transverse components have almost the same size and peak

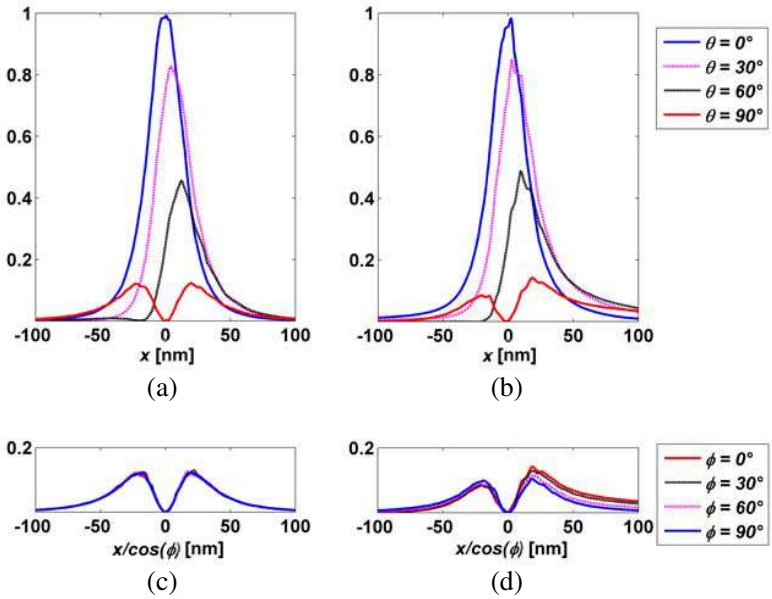

Figure 4. Line projections of the fluorescence distribution: (a) profile along x for a molecule with azimuthal angle $\phi = 0°$ and variable polar angle obtained with an axisymmetric probe under radially polarized excitation; (b) profile along x for a molecule with azimuthal angle $\phi = 0°$ and variable polar angle obtained with an asymmetric cut probe under x linearly polarized excitation; (c) profile along the straight line $x{\cdot}\tan(\phi)$ for a molecule with polar angle $\theta = 90°$ and variable azimuthal angle obtained with an axisymmetric probe under radially polarized excitation; (d) profile along the straight line $x \cdot \tan(\phi)$ for a molecule with polar angle $\theta = 90°$ and variable azimuthal angle obtained with an asymmetric cut probe under x linearly polarized excitation.

Table 1. Comparison of asymmetric probes with different geometric characteristics.

Probe type	Normalized longitudinal component	Normalized transverse components along x and y	FWHM (longitudinal) [nm]	FWHM (transverse) [nm]	Normalized total electric field intensity
Axisymmetric	0.994	0.123–0.125	31	82	1
Cut: 766 nm; 30°	0.986	0.105–0.143	30	74–80	1.478
Cut: 816 nm; 30°	0.974	0.095–0.194	31	65–77	0.281
Cut: 816 nm; 40°	0.944	0.101–0.193	32	62–80	0.499
Cut: 741 nm; 30°	0.997	0.097–0.161	30	60–77	2.109
Cut: 816 nm; 50°	0.963	0.119–0.180	31	63–84	2.026

intensity, the transverse component aligned along the input linear polarization is still slightly higher than the orthogonal component and marginally asymmetric (the two lobes are not identical as observed earlier in Figure 4) which accounts for the variations in the peak value and FWHM for the transverse components reported in Table 1. Such minor differences would only slightly affect the field distributions for variable ϕ, but are not likely to impair the high resolution mapping of the fluorescent molecules and the determination of their orientation.

So far only a linearly polarized excitation along the direction of the asymmetry has been considered. However, the behavior of such asymmetric probes is expected to vary as a function of the angle α between the direction of the input linearly polarized excitation and the direction of the asymmetry. As an example, we considered a molecule with longitudinal dipole moment and studied how the mapping of the

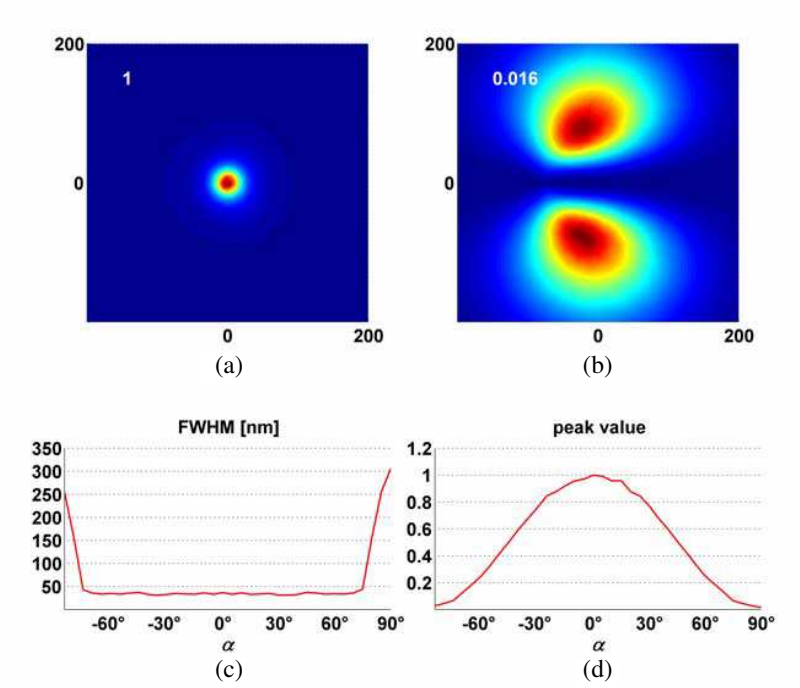

Figure 5. Mapping of a fluorescent molecule with longitudinal dipole moment with an asymmetric cut probe for variable α: (a) fluorescence map for $\alpha = 0°$; (b) fluorescence map for $\alpha = 90°$; (c) FWHM for variable α; (d) peak values for variable α (peak values normalized to the peak intensity for $\alpha = 0°$). The number in the corner in (a) and (b) reports the peak value normalized to the peak intensity for $\alpha = 0°$.

molecule varies with a transition from a situation of perfect alignment with respect to the asymmetry ($\alpha = 0°$) to complete misalignment, i.e., linearly polarized excitation orthogonal to the direction of the asymmetry ($\alpha = \pm 90°$). Figures 5(a) and (b) report the fluorescence maps for $\alpha = 0°$ and $\alpha = 90°$ and Figures 5(c) and (d) show the FWHM and peak value normalized to the one of $\alpha = 0°$ obtained for α variable from $-85°$ to $90°$ with an incremental step of $5°$. Plots refer to a cut probe with a cut angle of $30°$ and a cut height of 766 nm.

As the misalignment of the input polarization from the preferential direction of the asymmetry increases, both the peak value and the shape of the intensity pattern of the fluorescent molecule change. In particular, the peak value decreases and the distribution becomes gradually broader. This is due to the fact that, as α increases,

the asymmetry perceived by the input linearly polarized excitation progressively disappears and the probe near field distribution undergoes a transition from an essentially longitudinal polarization with higher intensity and strong confinement ($\alpha = 0°$) to a mainly linear polarization with low intensity and broad extension aligned along the direction of the input linear polarization ($\alpha = \pm 90°$). The latter is characterized by a dominant y polarized component, a weaker two-lobed z component and an even weaker four-lobed x component. In retrospect, the different behavior can be explained if recalling that a structure asymmetric along x appears symmetric for a y linearly polarized excitation, which brings about destructive interference of the excited SPPs, similarly to what happens for an axisymmetric structure under linearly polarized excitation.

In conclusion, the simulations confirm the impressive similarity between the axisymmetric probe with radially polarized excitation and the asymmetric probes under linearly polarized excitation along the direction of the asymmetry, which makes the asymmetric structures eligible to replace the axisymmetric probe for measurements on single fluorescent molecules, as long as the alignment of the input linear polarization with respect to the asymmetry is controllable and the direction of the asymmetry when the probe is mounted on the microscope is known. If such a condition is not met, the introduction of an adirectional asymmetry extended to all the spatial directions [34, 35] (and not oriented along one specific direction as is the case for the previously considered x-asymmetric structures) would be advisable. However, even in case of a directional asymmetry (i.e., with an asymmetry lying along one specific spatial direction, as the one examined in this paper), the mapping of the molecule does not dramatically change in both peak intensity and size for a broad range of misalignment of the input linear polarization from the preferential direction of the asymmetry, as shown in Figures 5(c) and (d).

4. CONCLUSIONS

The interaction of fluorescent molecules with fully metal-coated axisymmetric tips and with novel asymmetric tips has been thoroughly scrutinized. Our numerical analysis reveals that the fluorescence maps of molecules with different absorption dipole moments achieved with asymmetric tips under proper linearly polarized excitation are closely akin to those observed with an axisymmetric tip under radially polarized excitation. As single molecules serve as an effective point-like probe for the vectorial components of the near field distribution close to a SNOM tip, the similarity of the fluorescence distributions suggests

a substantial resemblance of such electric field components between the two probe structures. Both of them are characterized by a single-lobed longitudinal field component dominant over two almost identical two-lobed orthogonal transverse components. Hence, variations in the polar orientation of a fluorophore from mainly longitudinal to mainly transverse at constant azimuthal angle are mapped as a transition from a single-lobed to a two-lobed pattern, while changes in the azimuthal angle at constant polar orientation imply a simple rotation of the fluorescence distribution according to the azimuthal angle. This allows a more straightforward interpretation of the 3D orientation of single fluorescent molecules compared to aperture probes, characterized by a two-lobed longitudinal component and by orthogonal transverse components strongly unequal in magnitude and shape, with differences as high as two orders of magnitude.

Our simulations may be used in combination with experimental results to accurately determine the 3D dipole orientation of single fluorescent molecules measured with novel asymmetric probes and for the characterization of novel asymmetric probe structures using molecules with a prevalent known dipole moment. Although both axisymmetric fully metal-coated probes and asymmetric probes have been experimentally used in fluorescence experiments, a numerical modeling of the probe-fluorophore interaction was still missing. Our results could be helpful in the interpretation of the experimental data obtained with similar structures [32, 36, 37]. Moreover, the model could be extended to encompass measurements on quantum dots, for example by replacing the one-dimensional dipole with a two-dimensional one [38].

Noticeably, the numerical demonstration of the attainment of a strong longitudinal field component under linearly polarized excitation by the introduction of an asymmetry in an originally axisymmetric probe opens up interesting perspectives: longitudinal fields are essential not only for fluorescence measurements (especially for the high resolution imaging of fluorescent molecules with a mainly longitudinal dipole moment), but also for other potential applications like near field second-harmonic generation and Raman spectroscopy [39, 40]. Therefore, the possibility to generate them without resorting to a cumbersome radially polarized excitation would foster the development of new exciting horizons.

ACKNOWLEDGMENT

The authors gratefully acknowledge the support of the Swiss National Science Foundation (Project number 200021-115895).

REFERENCES

1. Dunn, R. C., "Near-field scanning optical microscopy," *Chem. Rev.*, Vol. 99, 2891–2927, 1999.
2. Van Zanten, T. S., A. Cambi, and M. F. Garcia-Parajo, "A nanometer scale optical view on the compartmentalization of cell membranes," *Biochimica and Biophysica Acta*, Vol. 1798, 777–787, 2010.
3. Hsu, J. W. P., "Near-field scanning optical microscopy studies of electronic and photonic materials and devices," *Materials Science and Engineering*, Vol. 33, 1–50, 2001.
4. Novotny, L. and B. Hecht, *Principles of Nano-optics*, Cambridge University Press, 2006.
5. Antosiewicz, T. J., M. Marciniak, and T. Szoplik, "On SNOM resolution improvement," *Photonic Crystals: Physics and Technology*, 217–238, Springer, Milan, 2008.
6. Mononobe, S., "Near-field optical fiber probes and the imaging applications," M. Ohtsu, (Ed.), *Springer Series in Optical Science*, Vol. 95, *Progress in Nano-electro-optics: Industrial Applications and Dynamics of the Nano-optical Systems*, 1–53, Springer, Berlin-Heidelberg, 2005.
7. Drezet, A., M. J. Nasse, S. Huant, and J. C. Woehl, "The optical near-field of an aperture tip," *Europhys. Lett.*, Vol. 66, No. 1, 41–47, 2004.
8. Liu, L. and S. He, "Design of metal-cladded near-field fiber probes with a dispersive body-of-revolution finite-difference time-domain method," *Appl. Opt.*, Vol. 44, No. 17, 3429–3437, 2005.
9. Michalski, K. A., "Complex image method analysis of a plane wave-excited subwavelength circular aperture in a planar screen," *Progress In Electromagnetics Research B*, Vol. 27, 253–272, 2011.
10. Hartschuh, A., "Tip-enhanced near-field optical microscopy," *Angewandte Chemie*, Vol. 47, 8178–8191, 2008.
11. Inouye, Y., "Apertureless metallic probes for near-field microscopy," S. Kawata (Ed.), *Springer Topics in Applied Physics*, Vol. 81, *Near-field Optics and Surface Plasmon Polaritons*, 29–48, Springer, Berlin-Heidelberg, 2001.
12. Chuang, C.-H. and Y.-L. Lo, "Signal analysis of apertureless scanning near-field optical microscopy with superlens," *Progress In Electromagnetics Research*, Vol. 109, 83–106, 2010.
13. Amin, A. S. N., M. Mirhosseini, and M. Shahabadi, "Modal analysis of multilayer conical dielectric waveguides for azimuthal in-

variant modes," *Progress In Electromagnetics Research*, Vol. 105, 213–229, 2010.

14. Ding, W., S. R. Andrews, and S. A. Maier, "Internal excitation and superfocusing of surface plasmon polaritons on a silver-coated optical fiber tip," *Phys. Rev. A*, Vol. 75, 063822-1–10, 2007.
15. Vaccaro, L., L. Aeschimann, U. Staufer, H. P. Herzig, and R. Dändliker, "Propagation of the electromagnetic field in fully coated near-field optical probes," *Appl. Phys. Lett.*, Vol. 83, No. 3, 584–586, 2003.
16. Bouhelier, A., J. Renger, M. R. Beversluis, and L. Novotny, "Plasmon-coupled tip-enhanced near-field optical microscopy," *J. of Microsc.*, Vol. 210, No. 3, 220–224, 2003.
17. Tortora, P., E. Descrovi, L. Aeschimann, L. Vaccaro, H. P. Herzig, and R. Dändliker, "Selective coupling of HE_{11} and TM_{01} modes into microfabricated fully metal-coated quartz probes," *Ultramicroscopy*, Vol. 107, 158–165, 2007.
18. Chen, W. and Q. Zhan, "Numerical study of an apertureless near field scanning optical microscope probe under radial polarization illumination," *Opt. Express*, Vol. 15, No. 7, 4106–4111, 2007.
19. Nakagawa, W., L. Vaccaro, H. P. Herzig, and C. Hafner, "Polarization mode coupling due to metal-layer modifications in apertureless near-field scanning optical microscopy probes," *J. of Comput. and Theor. Nanosci.*, Vol. 4, No. 3, 1–12, 2007.
20. Lotito, V., U. Sennhauser, and C. Hafner, "Effects of asymmetric surface corrugations on fully metal-coated scanning near field optical microscopy tips," *Opt. Express*, Vol. 18, No. 8, 8722–8734, 2010.
21. Lotito, V., U. Sennhauser, and C. Hafner, "Finite element analysis of asymmetric scanning near field optical microscopy probes," *J. of Comput. and Theor. Nanosci.*, Vol. 7, No. 8, 1596–1609, 2010.
22. Yatsui, T., K. Itsumi, M. Kourogi, and M. Ohtsu, "Metallized pyramidal silicon probe with extremely high throughput and resolution capability for optical near-field technology," *Appl. Phys. Lett.*, Vol. 80, No. 13, 2257–2259, 2002.
23. Betzig, E. and R. J. Chichester, "Single molecules observed by near-field scanning optical microscopy," *Science*, Vol. 262, No. 5138, 1422–1425, 1993.
24. Hollars, W. and R. C. Dunn, "Probing single molecule orientations in model lipid membranes with near-field scanning optical microscopy," *J. of Chem. Phys.*, Vol. 112, No. 18, 7822–7830, 2000.

25. Veerman, J. A., M. F. Garcia-Parajo, L. Kuipers, and N. F. van Hulst, "Single molecule mapping of the optical field distribution of probes for near-field microscopy," *J. of Microsc.*, Vol. 194, Nos. 2–3, 447–482, 1999.
26. Moerland, R. J., N. F. van Hulst, H. Gersen, and L. Kuipers, "Probing the negative permittivity perfect lens using near-field optics and single molecule detection," *Opt. Express*, Vol. 13, No. 5, 1604–1614, 2005.
27. Kulzer, F. and M. Orrit, "Single-molecule optics," *Ann. Rev. Phys. Chem.*, Vol. 55, 585–611, 2004.
28. García-Parajó, M. F., J.-A. Veerman, R. Bouwhuis, R. Vallée, and N. F. van Hulst, "Optical probing of single fluorescent molecules and proteins," *Chemphyschem*, Vol. 2, 347–360, 2001.
29. Van Hulst, N. F., J.-A. Veerman, M. Garcia-Parajo, and L. K. Kuipers, "Analysis of individual (macro) molecules and proteins using near-field optics," *J. of Chem. Phys.*, Vol. 112, No. 18, 7799–7810, 2000.
30. Van Hulst, N. F., M. F. Garcia-Parajo, M. H. P. Moers, J.-A. Veerman, and A. G. T. Ruiter, "Near-field fluorescence imaging of genetic material: Toward the molecular limit," *J. of Structural Biology*, Vol. 119, 222–231, 1997.
31. Ruiter, A. G. T., J. A. Veerman, M. F. Garcia-Parajo, and N. F. van Hulst, "Single molecule rotational and translational diffusion observed by near-field scanning optical microscopy," *J. Phys. Chem. A*, Vol. 101, 7318–7323, 1997.
32. Frey, H. G., C. Bolwien, A. Brandenburg, R. Ros, and D. Anselmetti, "Optimized apertureless optical near-field probes with 15 nm optical resolution," *Nanotechnology*, Vol. 17, 3105–3110, 2006.
33. Butter, J. Y. P. and B. Hecht, "Aperture scanning near-field optical microscopy and spectroscopy of single terrylene molecules at 1.8 K," *Nanotechnology*, Vol. 17, 1547–1550, 2006.
34. Lotito, V., U. Sennhauser, C. Hafner, and G.-L. Bona, "Fully metal-coated scanning near-field optical microscopy probes with spiral corrugations for superfocusing under arbitrarily oriented linearly polarized excitation," *Plasmonics*, Vol. 6, 327–336, 2011.
35. Lotito, V., U. Sennhauser, and C. V. Hafner, "Numerical analysis of novel asymmetric SNOM tips," *PIERS Online*, Vol. 7, No. 4, 394–400, 2011.
36. Frey, H. G., F. Keilmann, A. Kriele, and R. Guckenberger, "Enhancing the resolution of scanning near-field optical microscopy

by a metal tip grown on an aperture probe," *Appl. Phys. Lett.*, Vol. 81, No. 26, 5030–5032, 2002.

37. Taminiau, T. H., F. B. Segerink, R. J. Moerland, L. Kuipers, and N. F. van Hulst, "Near field driving of a optical monopole antenna," *J. Opt. A: Pure Appl. Opt.*, Vol. 9, S315–S321, 2007.
38. Li, Q., X.-J. Chen, Y. Xu, S. Lan, H.-Y. Liu, Q.-F. Dai, and L.-J. Wu, "Photoluminescence properties of CdSe quantum dots accompanied with rotation of the defocused wide-field fluorescence images," *J. Phys. Chem. C*, Vol. 114, 13427–13432, 2010.
39. Bouhelier, A., M. Beversluis, A. Hartschuh, and L. Novotny, "Near-field second-harmonic generation induced by local field enhancement," *Phys. Rev. Lett.*, Vol. 90, No. 1, 013903-1–4, 2003.
40. Hayazawa, N., Y. Saito, and S. Kawata, "Detection and characterization of longitudinal field for tip-enhanced Raman spectroscopy," *Appl. Phys. Lett.*, Vol. 85, No. 25, 6239–6241, 2004.